Fracture resistance of railway ballast rock under tensile and tear loads

A. Bahmani[a,b*] and S. Nemati[c]

[a]Department of Mechanical Engineering, McGill University, Montreal, QC H3A2K6, Canada
[b]Department of Mechanical and Mechatronics Engineering, University of Waterloo, 200 University Ave. West, Waterloo N2L3G1, Canada
[c]Centre for Infrastructure Engineering, Western Sydney University, Building Z, 56 Second Ave, Kingswood NSW 2747, Sydney, Australia

A R T I C L E I N F O	A B S T R A C T
	The influence of loading type on tensile and tearing fracture resistance of ballast rock was assessed using edge-notched diametrically compressed disc (ENDC) and edge-notched disc bend (ENDB) test geometries. The geometry of these two specimens was similar; however, their loading type (i.e., three-point bend and diametral compressive) was different affecting the geometry factors. The obtained pure tensile fracture toughness (K_{Ic}) using the ENDB test was higher than the ENDC test. In contrast to tensile fracture toughness, the pure tearing fracture toughness (K_{IIIc}) in the ENDC test was higher than the ENDB fracture test. The obtained experimental data were explained in terms of crack propagation path, since two distinct trajectories were observed for both configurations under tearing deformation.

1. Introduction

Rock materials in real practical fields can be loaded with complex state of stress resulting in tensile and tearing deformations. Different form of catastrophic failures can be happened under any of these loading conditions. The circumstance of ballast rock used in railways is a practical example in this case. Hence, it is essential to individually investigate the effect tensile and tearing loading on the onset of fracture in geo-materials. The framework of liner elastic fracture mechanics has usually been used for this purpose (e.g. Ayatollahi et al., 2017; Abbas et al. 2013; Alkan & Tutluoglu, 2016; Balme et al., 2004; Justo et al., 2021; Aliha et al., 2015, 2016, 2017; Saghafi et al., 2013; Saghafi and Monemian, 2010). Fracture toughness is a major inherent material property in the usage of fracture mechanics framework (Tahmoorian et al., 2017, 2018; Nemati & Tahmoorian, 2020). Disc shape configurations have often been employed to obtain fracture toughness of rocks (Fakhri et al., 2017; Shi et al., 2019; Aliha et al., 2010, 2013; Akbardoost and Rastin 2015; Akbardoost et al. 2017) because they can simply be extracted from the cylindrical or rod shape cores. Examples of such test samples include Brazilian discs (Wei et al., 2018; Wang & Wu, 2004; Aliha et al., 2010, 2018; Akbardoost et al. 2014), semi-circular discs (Aliha et al., 2010, 2018; Saghafi et al., 2010; Mirsayar et al., 2017), short-rod specimen (Barker, 1981; Ingraffea, 1984), and edge-cracked cylindrical specimen (Ouchterlony, 1990). These test specimens were employed to obtain tensile-sliding fracture toughness. Tearing fracture toughness also is another crack deformation that has rarely been studied for rock materials, especially ballast rock.

Examples of disc shape specimens used for tensile and tearing fracture toughness include edge-notched disc bend (ENDB) (Bahmani et al., 2021; Aliha et al., 2015b, 2016b, 2017b, 2017c, 2018b, Bidadi et al., 2020), and edge-notched diametrically compressed disc (ENDC) (Bahmani et al., 2021, 2019; Aliha et al., 2017c).

It has been explored that the magnitude of fracture toughens depends on both loading type and geometry of test sample (Aliha et al., 2017d, 2018, 2019). These dependencies have less been assessed for pure tearing fracture toughness. The individual influence of geometry and loading manner can be studied when one of them is fixed and the other varies. This specific testing condition can be provided using the ENDB and ENDC specimens because the geometry of these two specimens is the same while producing pure tearing deformation under two loading senarios (i.e., bending and compression). In this paper, we took advantage of the ENDB and ENDC specimens to assess the influence of loading manner on the measurement of pure tensile and tearing fracture toughness for ballast rock used in the railways.

2. Finite element modeling and results

The fracture toughness of a brittle material under pure tension and tearing can be described via the stress intensity factor (SIF) at the applied critical load. Individual geometry factors are required to measure the fracture toughness of a material subjected to different crack deformations and loading conditions. Therefore, we run many finite element models to compute the required geometry factors of the ENDB and ENDC specimens in obtaining pure tensile and tearing fracture toughness. Finite element (FE) code has mostly been used to compute these fracture parameters as a reliable and efficient tool. The J-integral method provided in ABAQUS software was used to simulate 3D models of ENDB and ENDC samples. Fig.1 shows meshed ENDB and ENDC specimens subjected to pure tensile and tearing loading conditions. There is an edge crack at one side of the main disc cutting through its diameter. The ENDB specimen was tested using a 3point bend setup while the ENDC specimen can diametrically be compressed via two plates. The main disc can be rotated about its axial axis; thus, the edge crack has an angle β (for the ENDB specimen) and α (for the ENDC specimen) relative to the loading lines. Where β or α is zero, pure tensile deformation can be achieved, while increasing β or α can create the combination of tensile and tearing or pure tearing conditions.

The main disc geometry was modeled with radius R=35 mm and thickness B=40 mm. Based on these two dimensions, other effective dimensions such as S (the distance between the bottom loading supports to the center point of the ENDB specimen) and a (crack depth or length) can be defined. In addition, the isotropic elastic properties of the models were Young's modulus= 70 GPa and Poisson's ratio=0.3. Three-dimensional quadratic elements were used at the crack tip to create the square root singularity of stress/strain field. The stress intensity factor under pure tensile deformation (K_I) and pure tearing (K_{III}) for both ENDC and ENDB tests are defined by Eq (1-4) (Bahmani et al., 2021). We first computed the stress intensity factors using ABAQUS and then calculated corresponding geometry factors (Y_I and Y_{III}) using the following equations.

$$K_{I\,(ENDB)} = \frac{3PS}{2RB^2}\sqrt{\pi a}\ Y_I(a/B, S/R, \beta) \tag{1}$$

$$K_{III\,(ENDB)} = \frac{3PS}{2RB^2}\sqrt{\pi a}\ Y_{III}(a/B, S/R, \beta) \tag{2}$$

$$K_{I\,(ENDC)} = \frac{P}{RB}\sqrt{\pi a}Y_I(a/B, \alpha) \tag{3}$$

$$K_{III\,(ENDC)} = \frac{P}{RB}\sqrt{\pi a}Y_{III}(a/B, \alpha) \tag{4}$$

in which P is the applied force; $Y_{I(ENDB)}$, $Y_{III(ENDB)}$, $Y_{I(ENDC)}$, and $Y_{III(ENDC)}$ are the geometry factors or non-dimensional forms of the corresponding values of stress intensity factors (i.e. $K_{I(ENDB)}$, $K_{III(ENDB)}$, $K_{I(ENDC)}$, and $K_{III(ENDC)}$, respectively).
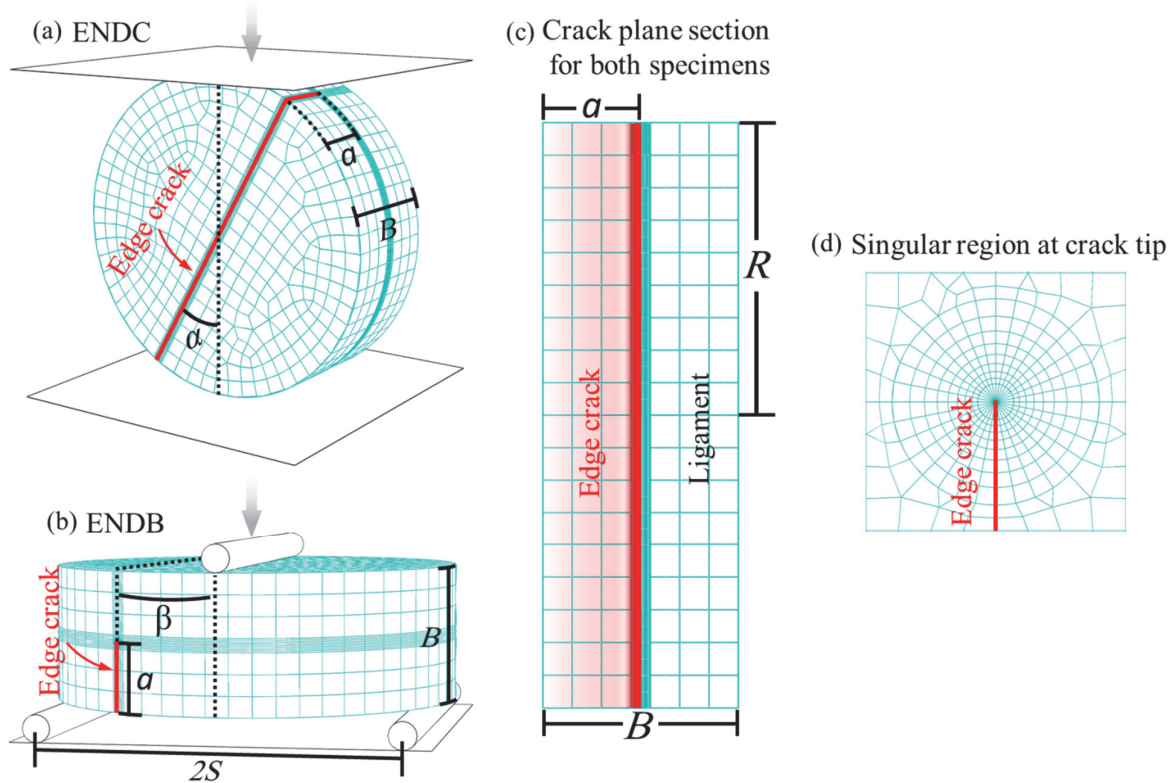

Fig. 1. (a) and (b) Meshed geometry and loading manners of the ENDC and ENDB fracture test specimens; (c) the section of cracked region of both specimens; (d) quadratic elements used for the square root singularity of stress/strain field at crack tip.

Since the crack front for both configurations is a continuous and straight line along the diameter of disc, depending on the location at the crack front, various SIFs are existed for each point. It has been assessed that stress intensity factor under sliding is zero at the center point of both specimens (Aliha et al., 2015c; Bahmani et al., 2021, 2017). While the maximum magnitude of stress intensity factor under pure tension and tearing is at the center point of both specimens. It has been showed that the center node in these two test configurations is the critical location for initiation and start of fracture (Aliha et al., 2015c; Bahmani et al., 2021). Therefore, the required geometry factors were obtained at the center point. When α and β is zero, both ENDB and ENDC samples produce pure tensile deformation. Pure tearing occurs when $\beta \approx 65°$ and $S/R = 0.925$ in the ENDB specimen and $\alpha \approx 18°$ for the ENDC specimen.

Suitable fracture parameter is the dimensionless SIF so-called geometry factor. Fig. 2. shows the variation of pure tensile and tearing geometry factors (Y_I and Y_{III}) versus the crack length (depth) ratio (a/B) for both the ENDC and ENDB specimens calculated using Eqs. (1-4).. Both Y_I and Y_{III} in the ENDC specimen are increased by extending crack length (depth) through the thickness. However, in the ENDB specimen, Y_I nonlinearly increases and Y_{III} linearly decreases as the function of crack length (depth) enlargement.
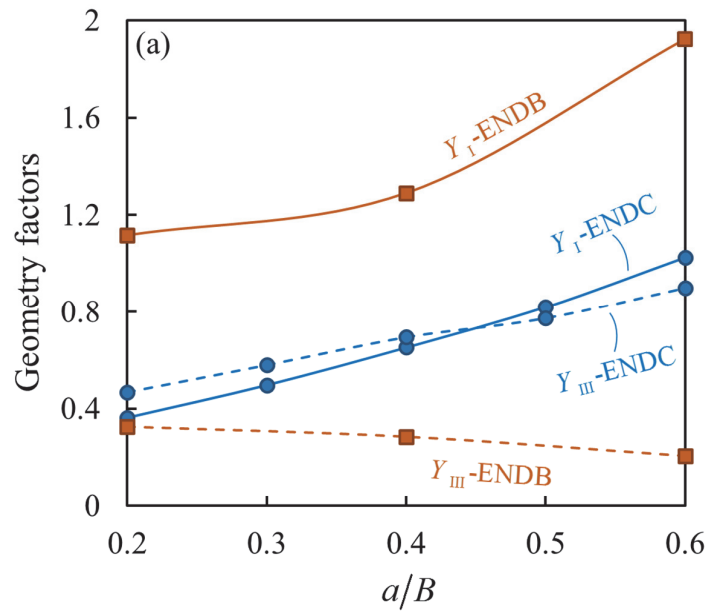
Fig. 2. Graphs of tensile and tearing mode geometry factors (i.e., Y_I and Y_{III}) as the function of crack length (depth) ratio (a/B) along thickness calculated at the center of the ENDC and ENDB samples.

The crack incline angle for the ENDB specimen under pure tension and tearing sequentially were $\beta = 0°$ and $\beta \approx 65°$ at $S/R = 0.925$. The ENDC specimen was under pure tension and tearing at $\alpha = 0°$ and $\alpha \approx 18°$, respectively.

3. K_{Ic} and K_{IIIc} experiments on rock and results

Pure tensile and tearing fracture toughness tests were implemented using the ENDB and ENDC specimens on railway ballast rock that is a granite material. Ten disc shape samples with diameter of $2R = 70$ mm and thickness of $B = 40$ mm were cut. An artificial pre-crack with 16 mm initial depth was cut along the diameter of main disc using a 0.4 mm thick rotary diamond saw blade. Fig. 3 (a and b). shows the ENDB specimen under three-point bend load and the ENDC specimen subjected to compression using rigid plates. Both loading configurations were fixed on a servo-hydraulic compression testing machine. The experiments were implemented with a 1 mm/min constant monotonic loading rate. Each case was repeated five times to reliably obtain the fracture loads. We then used the obtained fracture loads into Eq (1-4) to calculate fracture toughness values. Table 1 indicates the details of implemented fracture toughness tests on ENDB and ENDC samples.

Table 1. Geometrical and loading conditions, and fracture load (P) obtained for the tested samples under pure tension and pure tearing loads

Test sample	ENDB specimen				ENDC specimen		
Deformations	a/B	S/R	$B(degree)$	$P(N)$	a/B	α (degree)	$P(N)$
Pure tensile deformation	0.4	0.925	0°	9051 10500 11200 10300 10753	0.4	0°	15244 15032 14443 13061 13342
Pure tearing deformation	0.4	0.925	65°	13234 14720 18540 14061 12032	0.4	18°	16256 17670 17131 16421 18300

Figs. 3 (c-f) present the crack propagation trajectory of both tested samples under pure tensile and tearing loads. The fracture surface of both samples also indicate brittle type crack path for the tested granite rock. Similar to previous studies (Bahmani et al., 2017; Aliha et al., 2017c), the onset of fracture would happen at the center of both specimens. The crack path in both specimens is a mirror-type crack propagation by which both specimens were broken into two similar halves along the primary crack. However, the crack path of the ENDB specimen is different from the ENDC specimen under pure tearing. The crack path of the ENDB specimen is more similar to an anti-symmetric curvilinear pattern, initiating via a small degree of twist about the center of the specimen. This twist tends to be inclined through the crack front from the center to both corners of the disc. For the ENDC configuration, the crack propagation path is approximately mirror-type without any twist from the center to the half of the crack front. However, from the second half of the crack front to both corners, the crack trajectory is more similar to an anti-symmetric inclined twist, while it gradually increases about the center of the crack front. These figures demonstrate that the crack initiation direction may notably govern by the loading manner as well as tensile-tearing deformations at different location of crack front. Indeed, the crack trajectory in the ENDC specimen begins at the center of main disc with a remarkable smaller twist angle compared to the ENDB specimen. Therefore, in the ENDC specimen under pure tearing, the crack trajectory was not entirely self-similar through the crack plane. The crack path was begun with a slight angle from the center and propagated toward both endpoints of the main disc. The crack path slope tends to be greater from the half of the crack front, probably because of the effect of different tensile-tearing deformations that exist at the different crack front nodes or the corner point effects created due to applied compression force. In the same crack front position, the crack initiation angle for the ENDB sample is higher than the ENDC sample under pure tearing load. The crack initiation direction tends to be inclined by moving from pure tension to pure tearing deformations and from the center of disc toward the corners of disc samples. The crack path under pure tearing indicates an anti-symmetric trajectory about the center point of both ENDB and ENDC specimens.
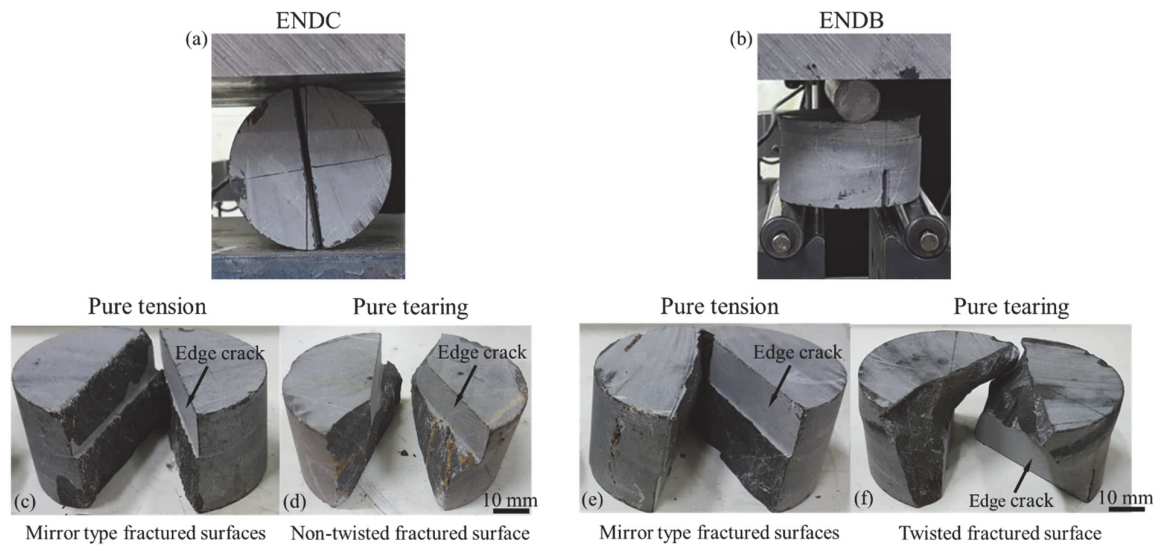

Fig. 3. Test configuration for (a) the ENDC specimen and (b) the ENDB specimen. Fracture trajectory of the ENDC specimen subjected to (c) pure tensile and (d) pure tearing loading conditions. Fracture trajectory of the ENDB specimen subjected to (e) pure tension and (f) pure tearing.

The observed fracture surfaces reveal that the a possible reason for such twisting fracture path is that the fracture would be started first from the center of disc and then propagated simultaneously from this location toward the corner nodes to create an anti-symmetric failure surface. Otherwise, if one assume any other location at the crack front as the crack initiation point, it is impossible to observe an anti-symmetric crack path relative to the center point of main disc. These conclusions and hypotheses have

also been recorded in the literature. (Aliha et al., 2015b, 2016b, 2017b, 2017c, 2018b; Bahmani et al., 2021, 2019).

Fig. 3 (a) indicates the pure tensile and pure tearing fracture toughness of both ENDC and ENDB specimens. The average pure tensile fracture toughness (K_{Ic}) obtained via the ENDC and ENDB samples are 1.6 MPa.m$^{0.5}$ and 1.47 MPa.m$^{0.5}$, respectively. While for pure tearing mode deformation, the average values of K_{IIIc} sequentially are 1.9 MPa.m$^{0.5}$ and 0.8 MPa.m$^{0.5}$ for the ENDC and ENDB specimens. The K_{Ic} value obtained via the ENDB test is higher than the ENDC test. In contrast, magnitude of K_{IIIc} obtained by the ENDC geometry is remarkably higher than the ENDB one. Fig.3 (b) shows the ratio between pure tearing fracture toughness (K_{IIIc}) and pure tensile fracture toughness (K_{Ic}) for each specimen. The ratio of K_{IIIc}/ K_{Ic} reveals that how loading manner affects the fracture resistance of the material under different tensile-tearing deformations. Pure tearing fracture toughness of ballast rock is relatively higher than its pure tensile fracture resistance under compression loading, while under bending, its pure tearing fracture toughness is noticeably lower than its pure tensile fracture resistance.
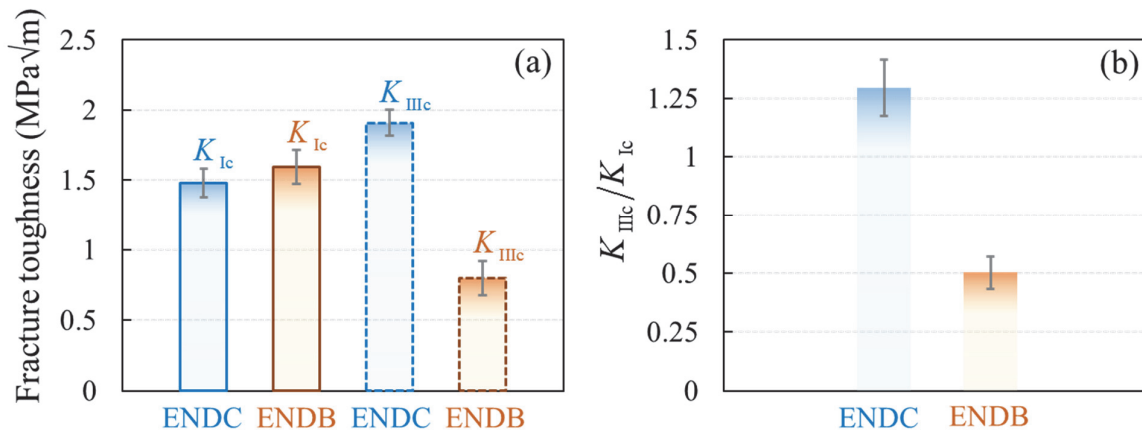

Fig. 4. (a) K_{Ic} and K_{IIIc} values obtained from ENDC and ENDB testing for ballast rock material; (b) the ratio of K_{IIIc} / K_{Ic} for both samples made of ballast rock

It has been assessed that fracture surface and trajectory, T-stress, Tz, and process zone size are the main reasons for these differences in pure tensile and pure tearing fracture toughness of these two specimens. These key player parameters are governed by the stress triaxiality or, in another word, the loading manner (Bahmani et al., 2021). The ENDC sample failed with a combined self-similar and twisting crack path, while the ENDB configuration was broken with an anti-symmetry twist through its entire fracture trajectory. Thus, the stress triaxiality constraint in the ENDC sample is greater than the ENDB sample under pure tearing loading condition. Likewise, both specimens had a similar crack path under the pure tensile loading condition; hence, they almost had the same stress triaxiality constraints. Thus, their pure tensile fracture toughness was restively close to each other (Bahmani et al., 2021).

4. General discussion and conclusion

Similar to tearing mode investigated in this study, there are many uncertainties regarding the mechanism governing pure sliding fracture toughness. Two different sliding fracture trajectories have been identified, including complete kinked fracture and straight crack growth. The magnitude of pure in-plane sliding mode fracture resistance of later is much greater than the former one (Bahmani et al., 2020; Bahrami et al., 2020; Backers et al., 2002, 2004). Therefore, it was demonstrated that the same scenario can occur for the pure tearing fracture mode. In the ENDB sample, the cracking trajectory was completely twisted; hence, the pure tearing fracture toughness value was lower than the ENDC, in which there was no fully twisted crack path at its entire crack front. It was shown that using the same geometry with two different loading manners, the pure tearing fracture toughness can be measured. Although the geometry

of ENDB and ENDC samples was similar, the difference in their loading type had notable influences on the values of geometry factors and fracture toughness.

Both specimens do have a long crack front by which a minimum plane-stain fracture toughness of the material can be measured. Both specimens did have a mirror-type and similar crack path under pure tensile loading condition, implying that both specimens are under nearly similar stress triaxiality constraints. However, the crack path of the ENDB sample under pure tearing loading condition was anti-symmetrically twisted, while in the ENDC sample was a combined straight and twisted propagation. The crack initiation angles for both specimens were distinct, meaning that the crack initiation and growth direction were dependent on the loading manner and are not necessarily similar for any given tensile-tearing deformations measured from different test specimens. Therefore, the fracture trajectory in engineering cases, including cutting rock masses, stability of slopes, tunnels, and mines, can noticeably be under the influence of loading manner even with identical geometry. Therefore, to assess any crack path of a fracture in geo-materials under the combination of tensile-tearing loads, the influence of loading manner needs to be considered.

Fracture resistance of rock masses against fracture propagation usually is required for engineering applications in this field. On one side, the minimum fracture load bearing has been required as an input parameter in designing and selecting drilling, cutting, fragmenting, and excavating tools. On the other side, the maximum fracture load bearing of the rock masses is needed to assess the onset of failures and collapses in the practical fields. Investigating the stability and integrity of underground rock structures and rock slopes containing pre-fractures are exemplary cases. The realistic rock masses are frequently under different crack mode deformations; therefore, an estimated resultant pure tearing fracture resistance must be quantified. However, according to the findings of the present research that is in good agreement with previous works available in the literature (Aliha et al., 2012), the fracture resistance of rocks obtained from laboratory test specimens is not a unique value and depends on the geometry and loading type. Thus, an upper and lower bound of fracture resistance can be identified for any given combined tensile-tearing deformations of rocks. These upper and lower fracture resistance bounds were presented for both pure tension and pure tearing modes using the capability of the ENDC and ENDB samples. These bounds are required to estimate a reliable magnitude of load bearing capacity for rock materials. The ENDC and ENDB samples were here recommended because conducting K_{Ic} and K_{IIIc} tests would be rapid and straightforward using field coring of these two specimens from cylindrical rock masses.

These obtained fracture toughness magnitudes can then be employed as the input design factors in practical rock engineering projects. The upper bound magnitudes measured via the ENDC specimen can be employed to identify the minimum cutting forces. For stability assessments of tunnels and mines, where the maximum resistance against the fracture propagation is required, the lower bound magnitudes measured by the ENDB specimen can be utilized as a safe design factor.

Both ENDB and ENDC samples and configurations can be considered as suitable test specimens to conduct K_{Ic} and K_{IIIc} tests on rock materials. Both specimens do have a simple main disc that can be easily subjected to pure tensile and pure tearing loading conditions using the conventional 3point bending or diametral compression setups. The main disc itself can be obtained and manufactured from cylindrical cores, while any rock material can commonly experience both bending and compression loads and deformations.

References

Abbas, S., Lecampion, B., & Prioul, R. (2013, February). Competition between transverse and axial hydraulic fractures in horizontal wells. In *SPE Hydraulic Fracturing Technology Conference*. Society of Petroleum Engineers.

Akbardoost, J., & Rastin, A. (2015). Comprehensive data for calculating the higher order terms of crack tip stress field in disk-type specimens under mixed mode loading. *Theoretical and Applied Fracture Mechanics*, *76*, 75-90.

Akbardoost, J., Ayatollahi, M. R., Aliha, M. R. M., Pavier, M. J., & Smith, D. J. (2014). Size-dependent fracture behavior of Guiting limestone under mixed mode loading. *International Journal of Rock Mechanics and Mining Sciences*, *71*, 369-380.

Akbardoost, J., Ghadirian, H. R., & Sangsefidi, M. (2017). Calculation of the crack tip parameters in the holed-cracked flattened Brazilian disk (HCFBD) specimens under wide range of mixed mode I/II loading. *Fatigue & Fracture of Engineering Materials & Structures*, *40*(9), 1416-1427.

Aliha, M. M., Behbahani, H., Fazaeli, H., & Rezaifar, M. H. (2014). Study of characteristic specification on mixed mode fracture toughness of asphalt mixtures. *Construction and Building Materials*, *54*, 623-635.

Aliha, M. R. M., & Bahmani, A. (2017b). Rock fracture toughness study under mixed mode I/III loading. *Rock Mechanics and Rock Engineering*, *50*(7), 1739-1751.

Aliha, M. R. M., Ayatollahi, M. R., & Akbardoost, J. (2012). Typical upper bound–lower bound mixed mode fracture resistance envelopes for rock material. *Rock mechanics and rock engineering*, *45*(1), 65-74.

Aliha, M. R. M., Ayatollahi, M. R., Smith, D. J., & Pavier, M. J. (2010). Geometry and size effects on fracture trajectory in a limestone rock under mixed mode loading. *Engineering Fracture Mechanics*, *77*(11), 2200-2212.

Aliha, M. R. M., Bahmani, A., & Akhondi, S. (2015). Fracture and fatigue analysis for a cracked carabiner using 3D finite element simulations. *Strength of Materials*, *47*(6), 890-902.

Aliha, M. R. M., Bahmani, A., & Akhondi, S. (2015b). Determination of mode III fracture toughness for different materials using a new designed test configuration. *Materials & Design*, *86*, 863-871.

Aliha, M. R. M., Bahmani, A., & Akhondi, S. (2015c). Numerical analysis of a new mixed mode I/III fracture test specimen. *Engineering Fracture Mechanics*, *134*, 95-110.

Aliha, M. R. M., Bahmani, A., & Akhondi, S. (2016). Mixed mode fracture toughness testing of PMMA with different three-point bend type specimens. *European Journal of Mechanics-A/Solids*, *58*, 148-162.

Aliha, M. R. M., Bahmani, A., & Akhondi, S. (2016b). A novel test specimen for investigating the mixed mode I+ III fracture toughness of hot mix asphalt composites–Experimental and theoretical study. *International Journal of Solids and Structures*, *90*, 167-177.

Aliha, M. R. M., Berto, F., Bahmani, A., & Gallo, P. (2017). Mixed mode I/II fracture investigation of Perspex based on the averaged strain energy density criterion. *Physical Mesomechanics*, *20*(2), 149-156.

Aliha, M. R. M., Linul, E., Bahmani, A., & Marsavina, L. (2018b). Experimental and theoretical fracture toughness investigation of PUR foams under mixed mode I+ III loading. *Polymer Testing*, *67*, 75-83.

Aliha, M. R. M., Mahdavi, E., & Ayatollahi, M. R. (2017d). The influence of specimen type on tensile fracture toughness of rock materials. *Pure and Applied Geophysics*, *174*(3), 1237-1253.

Aliha, M. R. M., Mahdavi, E., & Ayatollahi, M. R. (2018). Statistical analysis of rock fracture toughness data obtained from different chevron notched and straight cracked mode I specimens. *Rock Mechanics and Rock Engineering*, *51*(7), 2095-2114.

Aliha, M. R. M., Mousavi, S. S., Bahmani, A., Linul, E., & Marsavina, L. (2019). Crack initiation angles and propagation paths in polyurethane foams under mixed modes I/II and I/III loading. *Theoretical and Applied Fracture Mechanics*, *101*, 152-161.

Aliha, M. R. M., Sarbijan, M. J., & Bahmani, A. (2017c). Fracture toughness determination of modified HMA mixtures with two novel disc shape configurations. *Construction and Building Materials*, *155*, 789-799.

Alkan, U., & Tutluoglu, L. (2016, June). Investigation of Beam Specimen Geometries Under Four-Point Asymmetric Bending for Shear Mode Fracture Toughness Measurements of Rocks. In *50th US Rock Mechanics/Geomechanics Symposium*. OnePetro.

Ayatollahi, M., Berto, F., Campagnolo, A., Gallo, P., & Tang, K. (2017). Review of local strain energy density theory for the fracture assessment of V-notches under mixed mode loading. *Engineering Solid Mechanics*, *5*(2), 113-132.

Backers, T., Stephansson, O., & Rybacki, E. (2002). Rock fracture toughness testing in Mode II—punch-through shear test. *International Journal of Rock Mechanics and Mining Sciences*, *39*(6), 755-769.

Bahmani, A., Aliha, M. R. M., & Berto, F. (2017). Investigation of fracture toughness for a polycrystalline graphite under combined tensile-tear deformation. *Theoretical and Applied Fracture Mechanics*, *90*, 53-64.

Bahmani, A., Aliha, M. R. M., Sarbijan, M. J., & Mousavi, S. S. (2020). An extended edge-notched disc bend (ENDB) specimen for mixed-mode I+ II fracture assessments. *International Journal of Solids and Structures*, *193*, 239-250.

Bahmani, A., Farahmand, F., Ataei, F., & Aliha, M. R. M. (2019). Mixed mode I/III fracture parameters for edge-notched diametrically compressed disc specimen. *Material Design & Processing Communications*, *1*(6), e86.

Bahmani, A., Farahmand, F., Janbaz, M. R., Darbandi, A. H., Ghesmati-Kucheki, H., & Aliha, M. R. M. (2021). On the comparison of two mixed-mode I+ III fracture test specimens. *Engineering Fracture Mechanics*, *241*, 107434.

Bahrami, B., Nejati, M., Ayatollahi, M. R., & Driesner, T. (2020). Theory and experiment on true mode II fracturing of rocks. *Engineering Fracture Mechanics*, *240*, 107314.

Balme, M. R., Rocchi, V., Jones, C., Sammonds, P. R., Meredith, P. G., & Boon, S. (2004). Fracture toughness measurements on igneous rocks using a high-pressure, high-temperature rock fracture mechanics cell. *Journal of Volcanology and Geothermal Research*, *132*(2-3), 159-172.

Barker, L. M. (1981). Short rod and short bar fracture toughness specimen geometries and test methods for metallic materials. In *Fracture Mechanics*. ASTM International.

Bidadi, J., Akbardoost, J., & Aliha, M. R. M. (2020). Thickness effect on the mode III fracture resistance and fracture path of rock using ENDB specimens. *Fatigue & Fracture of Engineering Materials & Structures*, *43*(2), 277-291.

Fakhri, M., Amoosoltani, E., & Aliha, M. R. M. (2017). Crack behavior analysis of roller compacted concrete mixtures containing reclaimed asphalt pavement and crumb rubber. *Engineering Fracture Mechanics*, *180*, 43-59.

Ingraffea, A. R., Gunsallus, K. L., Beech, J. F., & Nelson, P. P. (1984). A short-rod based system for fracture toughness testing of rock. In *Chevron-notched specimens: testing and stress analysis*. ASTM International.

Justo, J., Castro, J., & Cicero, S. (2021). Application of the Theory of Critical Distances for the Fracture Assessment of a Notched Limestone Subjected to Different Temperatures and Mixed Mode with Predominant Mode I Loading Conditions. *Rock Mechanics and Rock Engineering*, 1-20.

Mirsayar, M., Shi, X., & Zollinger, D. (2017). Evaluation of interfacial bond strength between Portland cement concrete and asphalt concrete layers using bi-material SCB test specimen. *Engineering Solid Mechanics*, *5*(4), 293-306.

Nemati, S., & Tahmoorian, F. (Eds.). (2020). *Sandy Materials in Civil Engineering: Usage and Management*. BoD–Books on Demand.

Ouchterlony, F. (1990). Fracture toughness testing of rock with core based specimens. *Engineering Fracture Mechanics*, *35*(1-3), 351-366.

Saghafi, H., & Monemian, S. (2010). A new fracture toughness test covering mixed-mode conditions and positive and negative T-stresses. *International journal of fracture*, *165*(1), 135-138.

Saghafi, H., Ayatollahi, M. R., & Sistaninia, M. (2010). A modified MTS criterion (MMTS) for mixed-mode fracture toughness assessment of brittle materials. *Materials Science and Engineering: A*, *527*(21-22), 5624-5630.

Saghafi, H., Zucchelli, A., & Minak, G. (2013). Evaluating fracture behavior of brittle polymeric materials using an IASCB specimen. *Polymer testing*, *32*(1), 133-140.

Shi, X., Mirsayar, M., Mukhopadhyay, A., & Zollinger, D. (2019). Characterization of two-parameter fracture properties of portland cement concrete containing reclaimed asphalt pavement aggregates by semicircular bending specimens. *Cement and Concrete Composites*, *95*, 56-69.

Tahmoorian, F., Samali, B., Tam, V. W., & Yeaman, J. (2017). Evaluation of mechanical properties of recycled material for utilization in asphalt mixtures. *Applied Sciences*, *7*(8), 763.

Tahmoorian, F., Samali, B., Yeaman, J., & Crabb, R. (2018). The use of glass to optimize bitumen absorption of hot mix asphalt containing recycled construction aggregates. *Materials*, *11*(7), 1053.

Wang, Q. Z., & Wu, L. Z. (2004). The flattened Brazilian disc specimen used for determining elastic modulus, tensile strength and fracture toughness of brittle rocks: experimental results. *International Journal of Rock Mechanics and Mining Sciences*, *41*, 26-30.

Wei, M. D., Dai, F., Xu, N. W., Liu, Y., & Zhao, T. (2018). A novel chevron notched short rod bend method for measuring the mode I fracture toughness of rocks. *Engineering Fracture Mechanics*, *190*, 1-15.